Colpitts Oscillator: A New Criterion of Energy Saving for High Performance Signal Sources

Anisha M. Apte
BTU Cottbus, Germany

Ajay K. Poddar
Synergy Microwave, NJ, USA

Ulrich L. Rohde
BTU Cottbus, Germany

Enrico Rubiola
FEMTO-ST Inst., France

Abstract—This paper describes a new criterion for designing power-efficient signal sources for the application in frequency generating and frequency controlled electronic circuits and systems. The novel approach is based on PI (phase-injection) and MC (mode-coupling) techniques for improving the DC-RF conversion efficiency (η) without degrading the PN (phase noise) and FOM (figure-of-merit) performances. Conventionally, Colpitts oscillator topology is known for low PN signal sources. With a systematic approach to the Colpitts oscillator this paper provides information for an optimized design and the resulting phase noise performances for both low quality factor (example: planar transmission line resonator based energy storing tank circuit) and high quality factor (example: crystal resonator based energy storing devices) based frequency generating sources.

Keywords—FOM, Mode-Couplin, Phase-Injection, PN

I. INTRODUCTION

The PN (phase noise) and DC-to-RF conversion efficiency (η) parameters are critical in setting the performance limits of time keeping and modern communication systems. Modern communication systems need oscillators as part of the design. In general, oscillator PN depends on Q (quality factor) of the energy storing device frequently called resonator tank circuit and the applied DC-bias (voltage/current) condition.

Colpitts oscillator topology is known for high frequency low phase noise signal sources, it comes in 3-flavors. Figure (1a), shows the conventional circuit configuration. This type of circuit is based on Edwin Henry Colpitts known for his invention of this oscillator and hence carries his name [1]. It uses a capacitive voltage divider and an inductor. In reality this simple circuit is not used but rather a derivation of this. This is shown in Figure (1b). The advantage of this circuit is that, the values for C_1 and C_2 are fixed and the frequency change occurs by changing C_3. If the frequency of Figure (1a) needs to be changed, a better choice is to vary the inductor L. His colleague Ralph Hartley [2] invented an inductive coupling oscillator. The advantage of such an oscillator having capacitors C_1 and C_2 replaced with a tap of the inductor has been used together with helical resonators. The frequency tuning is achieved purely capacitive. To minimize loading, the transistor of choice here is a FET, which has very high input impedance and provides minimum loading to the circuit. The disadvantage is that this circuit, using junction FETs, is limited to about 400 MHz. The transition frequency f_T is about 500MHz. FETs can also be used in the Colpitts oscillator as shown in Figure (1a), because of relatively lower loading than the bipolar transistor. The drawback of Figure (1a) is the heavy loading of the tuned circuit by the transistor. The circuit shown

in Figure (1b) is frequently referred to as the Clapp-Gouriet circuit [3]. At frequencies below 1GHz, both GaAs FETs and CMOS FETs are not a good choice because of their high flicker noise contribution. For the circuit of Figure (1b), it is theoretically possible to have L and C_3 in resonance in which case the oscillator will cease to work. It is important to note here that the same circuit topology is used also for crystal oscillators; here the inductor L is replaced by the crystal. The crystal is a series combination of L, C, and R with $Q = \omega L/R$. In practice the product of crystal Q and frequency is a constant. For 5 MHz, a typical Q of 2.5×10^6 is possible, resulting in a product of 12.5×10^{12}. If this is scaled to a crystal oscillator operating at 100MHz, the Q would be 125000. Manufacturers typically guarantee value of Q greater than 100000. Again, this crystal oscillator also falls into the category of Colpitts oscillator. A third variation is shown in Figure (1c). Here we have a parallel tuned circuit which is coupled loosely to the transistor. This circuit is found when building oscillators using ceramic resonator (CR) and SAW resonator oscillator. Figure (2) shows the typical 1 GHz CRO (ceramic resonator oscillator) [4].

This paper presents the new criterion of designing high efficiency oscillators with a discussion on resonator dynamics, DC-RF conversion efficiency (η) and oscillator FOM.
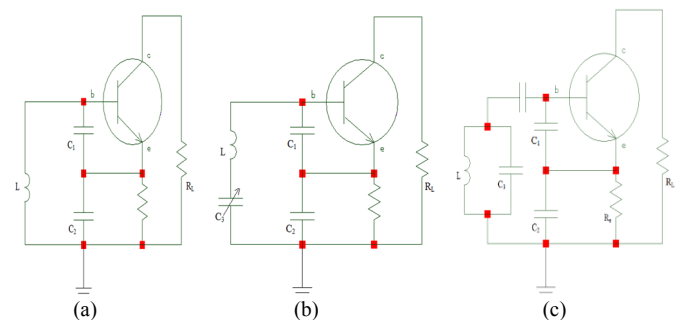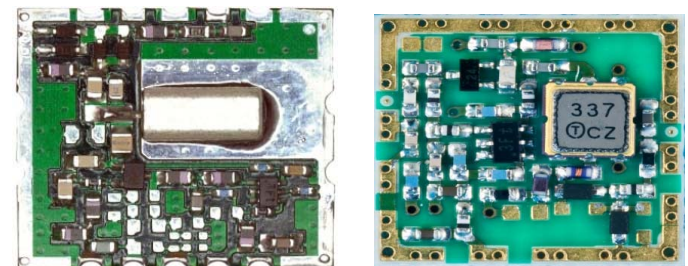

Fig. 1: Colpitts Configurations: (a) Conventional type, (b) Modified Colpitts (Clapp-Gouriet) Configuration and (c) Modified Colpitts Oscillator]

(a) 1 GHz CRO   (b) 1 GHz SAW Oscillator
Fig. 2: Layout of 1GHz Colpitts Oscillator: (a) CRO, (b) SAW oscillator [4]

II. Energy Storing Device: Resonator Elements

Resonators are considered as an energy storing element in oscillator circuits. Their broad classifications are based upon their principle of operations [4]. In this paper two types of resonators are discussed: planar transmission line resonator for tunable signal sources and crystal resonator for reference frequency sources applications.

A. Planar Transmission Line Resonator

Standard IC (integrated circuits) are planar circuits, therefore planar resonator based signal source is preferred choice. But planar resonator, for an example transmission line resonator offers low Q (quality factor) as compared to cavity resonator, resulting poor phase noise performance. Recent research work describes the methodology to improve the Q (quality factor) of metamaterial inspired planar resonator, but metamaterial resonator exhibits higher insertion loss and limited tuning capability [4]. In this paper, transmission line resonator network is reported in which Q factor can be improved by electromagnetic coupling. Figure (3) shows the typical capacitive coupling mechanism between two identical resonators (parallel tuned LCR). The resonator Q factor depends on the rate of change of the phase shift, given by [4]

$$\varphi = \tan^{-1}\left[\frac{\left(\frac{[R_P^2(1-\omega^2 LC)^2 - \omega^2 L^2]}{\omega^3 R_P^2 L^2 \beta C} - \frac{2R_P(1-\omega^2 LC)}{R_P \omega L}\right)}{\left(\frac{2}{R_P} - \frac{2R_P(1-\omega^2 LC)}{\omega^2 LR_P^2 \beta C}\right)}\right] \quad (1)$$

where 'β' is defined as the coupling factor, determined by the ratio of the series coupling capacitor (C_c) to the resonator capacitor (C). From (1), the Q factor of the capacitive coupled resonator network as shown in Figure (3) is given by

$$Q_L = [Q_{coupled}(\omega)]_{\omega=\omega_0} = \frac{\omega_0}{2}\left[\frac{\partial\phi}{\partial\omega}\right] \cong \frac{2Q_0(1+\beta)}{(1+Q_0^2\beta^2)} \Rightarrow \left[\frac{2Q_0(1+\beta)}{(1+Q_0^2\beta^2)}\right]_{\beta<<1} \approx 2Q_0 \quad (2)$$

where Q_0 is the unloaded quality factor of the resonator.

From (1) and (2), for weak coupling ($\beta <<1$), attenuation is high due to low value of series coupling capacitor (C_c), resulting in the large value of Z_c (Fig. 3). Therefore, there is a trade-off between doubling the Q factor and the permissible attenuation required for achieving optimum phase noise performance. In addition to this, manufacturing the lower value of the coupling capacitor at high frequency is challenging due to packaged parasitics and tolerances of the components.
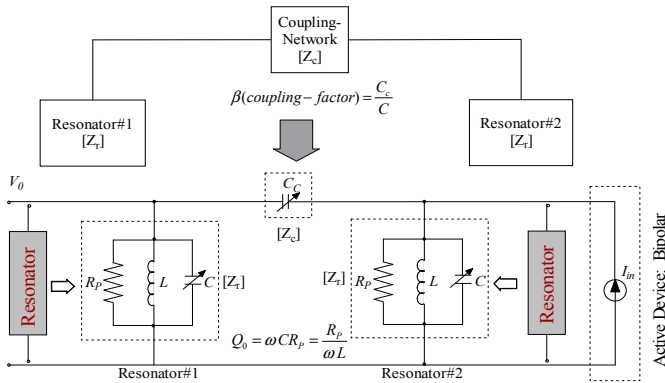
Therefore, coupling without employing the lumped coupling element (C_c) is preferred at high frequency. Figure (4) shows the typical self-coupled planar resonators, which is a parallel combination of two open-stubs with different lengths l_1 and l_2 ($l_{1,2}=\lambda_0/4\pm\Delta l$, λ_0 is wavelength at a resonant frequency) for the realization of coupling mechanism without the insertion of lumped coupling element. As shown in Figure (4), two unequal open-stub transmission line resonators exhibit resonant frequencies below and above f_0 in which length of resonators are symmetrically offset by the amount $\pm\Delta l$ ($\Delta l<<\lambda_0$). The coupling factor β can be controlled by varying the value of Δl without using the lumped coupling capacitor. The Q factor of this resonator can be evaluated based on input admittance $Y_i(\omega)$.

The input admittance $Y_i(\omega)$ of the self-coupled planar stubs-tuned resonator (Fig.4), and equivalent lumped values of the components (R_P, C_p, L_p) can be described by

$$Y_i(\omega) = G_i(\omega) + jB_i(\omega) \Rightarrow Z_i = \frac{1}{Y_i(\omega)} \quad (3)$$

$$Y_i(\omega) = Y_0\{\tanh[\gamma(\omega)l_1] + \tanh[\gamma(\omega)l_2]\} \quad (4)$$

$$Y_i(\omega) \cong \alpha(\omega)Y_0\left[\frac{l_1}{\cos^2(\omega l_1/v_p)} + \frac{l_2}{\cos^2(\omega l_2/v_p)}\right] + jY_0\left[\tan\left(\frac{\omega l_1}{v_p}\right) + \tan\left(\frac{\omega l_2}{v_p}\right)\right] \quad (5)$$

$$G_i(\omega) \cong \frac{\alpha(\omega)}{Z_0}\left[\frac{l_1}{\cos^2(\omega l_1/v_p)} + \frac{l_2}{\cos^2(\omega l_2/v_p)}\right] \quad (6)$$

$$B_i(\omega) \cong \frac{1}{Z_0}\left[\tan\left(\frac{\omega l_1}{v_p}\right) + \tan\left(\frac{\omega l_2}{v_p}\right)\right] \quad (7)$$

$$\varphi = \tan^{-1}\left[\frac{B_i(\omega)}{G_i(\omega)}\right] = \tan^{-1}\left\{\frac{\left[\tan\left(\frac{\omega l_1}{v_p}\right) + \tan\left(\frac{\omega l_2}{v_p}\right)\right]}{\alpha(\omega)\left[\frac{l_1}{\cos^2(\omega l_1/v_p)} + \frac{l_2}{\cos^2(\omega l_2/v_p)}\right]}\right\} \quad (8)$$

where Y_0, Z_0, v_p, φ, $\gamma(\omega)$, $G_i(\omega)$, and $B_i(\omega)$, are the characteristic admittance, characteristic impedance, phase velocity, phase shift, propagation constant, input conductance, input susceptance, respectively. From (6), R_p can be given by

$$R_p(\omega_0) = \frac{1}{G_i(\omega_0)} \cong \frac{Z_0}{\alpha(\omega_0)}\left[\frac{l_1}{\cos^2(\omega_0 l_1/v_p)} + \frac{l_2}{\cos^2(\omega_0 l_2/v_p)}\right]^{-1} \quad (9)$$

From (5) and (7), C_p and L_p can be given by [Fig.4]

$$C_p = \frac{1}{2}\left[\frac{\partial B_i(\omega)}{\partial\omega}\right]_{\omega=\omega_0} = C_p(\omega_0) = \frac{1}{2Z_0 v_p}\left[\frac{l_1}{\cos^2(\omega_0 l_1/v_p)} + \frac{l_2}{\cos^2(\omega_0 l_2/v_p)}\right] \quad (10)$$

$$L_p(\omega_0) = \frac{1}{\omega_0^2 C_p} \quad (11)$$

Fig.3 A typical simplified equivalent capacitive coupled resonator oscillator

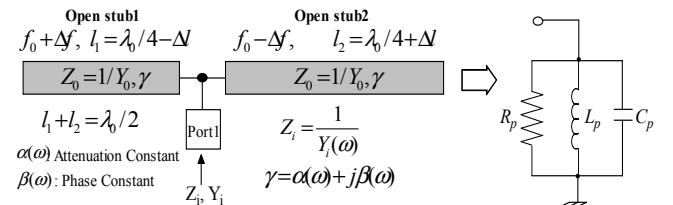

Fig.4 A typical example of self-coupled open-stubs resonator ($l_{1,2}=\lambda_0/4\pm\Delta l$)
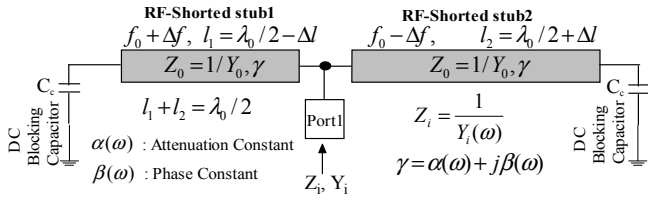
Fig.5.A typical example of self-coupled shorted-stubs resonator ($l_{1,2}=\lambda_0/2\pm\Delta l$)

From (9), (10), and (11), β and Q factor can be given by

$$\beta \cong \frac{\sin^2(\frac{2\pi}{\lambda_0}\Delta l)}{\alpha(\omega_0)[l_1+l_2]} = \frac{2\sin^2(\frac{2\pi}{\lambda_0}\Delta l)}{\alpha(\omega_0)\lambda_0} \quad (12)$$

$$Q_0 = \frac{R_p}{\omega_0 L_P} = R_p \omega_0 C_p \Rightarrow Q_0 \cong \frac{\pi}{2\alpha(\omega_0)[l_1+l_2]} = \frac{\pi}{\alpha(\omega_0)\lambda_0} = \frac{\beta(\omega_0)}{2\alpha(\omega_0)} \quad (13)$$

$$Q_L = [Q_{coupled}(\omega)]_{\omega=\omega_0} = \frac{\omega_0}{2}\left[\frac{\partial\phi}{\partial\omega}\right] \cong \frac{Q_0\alpha(\omega_0)[l_1+l_2]}{\left[\alpha(\omega_0)[l_1+l_2]+\sin^2(\frac{2\pi}{\lambda_0}\Delta l)\right]} \cong \frac{Q_0}{1+\beta} \quad (14)$$

From (9)-(14), it can be seen that R_p, C_p, L_p, β, and Q_L are dependent on the value of the offset length $\pm\Delta l$ of the open-stubs tuned resonators.

Figure (5) shows the self-coupled shorted–stubs which is a parallel combination of two unequal shorted-stubs, having different lengths l_1 and l_2 ($l_{1,2}=\lambda_0/2\pm\Delta l$) respectively, where λ_0 is a wavelength at a resonant frequency. For comparative analysis and better understanding about the open stubs self-coupled planar resonators, shorted stubs self-coupled resonators are discussed with respect to the resonator characteristics and parameters. The two unequal planar shorted-stubs exhibit resonant frequencies below and above f_0, in which length of the resonators are symmetrically offset by the amount $\pm\Delta l$ ($\Delta l<<\lambda_0$) for realization of coupling mechanism without the insertion of lumped element.

As illustrated in Figure (5), shorted-stubs are terminated with capacitors for dc blocking that can be removed when resonator is not dc-biased. The resonant characteristic is basically similar to the open-stubs resonators ($l_{1,2}=\lambda_0/4\pm\Delta l$), the resonator parameters (unloaded Q: Q_0, loaded Q: Q_L, and coupling factor: β) of shorted-stubs ($l_{1,2}=\lambda_0/2\pm\Delta l$) is given by

$$Q_0 \cong \frac{\pi}{\alpha(\omega_0)\lambda_0} = \frac{\beta(\omega_0)}{2\alpha(\omega_0)}, \quad \beta \cong \frac{\sin^2(\frac{2\pi}{\lambda_0}\Delta l)}{\alpha(\omega_0)[l_1+l_2]}, \quad Q_L = \frac{Q_0}{1+\beta} \quad (15)$$

Figure (6) demonstrates the circuit of 2488 MHz coupled shorted stub tuned resonator based oscillator/VCO for giving brief insight into the reduction of the phase noise with respect to the uncoupled single shorted-stub resonator oscillator/VCO. The measured DC-RF conversion efficiency of the oscillator circuit shown in Figure (6) is less than 5 % (4.2%) because of losses (radiation, higher order modes, harmonics) and also structure is sensitive to changes in the surrounding environment causing them to become microphonics, thereby, sensitive to phase hits. In order to solve the problem of microphonics and DC-RF conversion efficiency, the modified oscillator circuit is realized in stripline domain that provides self-shielding due to their dual ground plane. DC-to-RF conversion efficiency is related to the fundamental signal RF output power and DC power consumption, which can be described by

$$\eta_{efficiency} = \frac{P(\omega_0)}{P_{DC}} = \frac{P(\omega_0)}{V_{DC}\times I_{DC}} \quad (16)$$

where $\eta_{efficiency}$ is the DC-to-RF conversion efficiency, $P(\omega_0)$ is the RF output power of the fundamental signal and P_{DC} is DC power consumption.
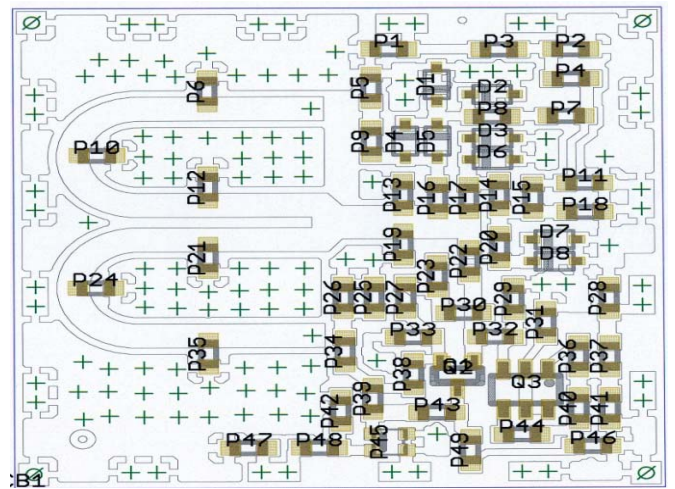
For higher conversion efficiency $\eta_{efficiency}$, oscillator circuit topology should be in such a way that it operates at low DC power and at the same time lower harmonics strengths, resulting maximum RF O/P power at fundamental frequency. The expression of the RF O/P power for a typical oscillator can be described in terms of the higher order harmonics as

$$P_{out} = V_0 I_0 + \frac{1}{2}V_1 I_1 \cos\theta_1 + \frac{1}{2}V_2 I_2 \cos\theta_2 + \cdots \frac{1}{2}V_n I_n \cos\theta_n \quad (17)$$

where V_1, I_1, V_2 I_2, and V_n, I_n, are the amplitudes of the voltage and currents of the fundamental, second and n^{th} harmonic components respectively; angle θ_1, θ_2, and θ_n are the phase angles between the voltage and the current of the respective harmonic components present at the output node of the oscillator circuit.
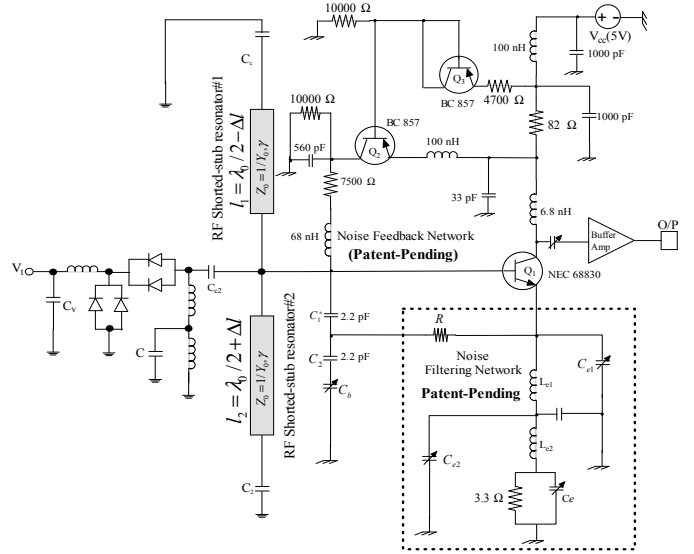
(a) Schematic self-coupled shorted-stubs resonator oscillator

(b) Layout of self-coupled shorted-stubs microstripline resonator oscillator

Fig.6. Typical 2488MHz planar resonator oscillator: (a) schematic, and (b) layout

From (17), DC-RF conversion efficiency (η) can be maximized by suppressing higher order harmonics. Figures (7) and (8) show the layout and phase noise plot of tunable oscillator (1200MHz-2450 MHz) using printed coupled resonator in stripline configuration. The measured phase noise for a carrier frequency 1.7 GHz is typically –120dBc/Hz at 10 kHz offset from the carrier with 15.38% DC-to-RF conversion efficiency. The measured RF output power at fundamental frequency 'f_0'is typically 10dBm for a given operating DC bias condition (V_{DC} = 5V, I_{DC} = 13mA). Table 1 shows the recent published papers on tunable wideband voltage controlled oscillator and compares this work based on DC-RF conversion efficiency, phase noise and FOM (figure of merit) at 1 MHz offset from the carrier [8]-[14]. As shown in Table 1, this work demonstrated the tunable octave band VCO (1200 MHz-2400 MHz) that exhibits 15.38 % DC-RF conversion with measured phase noise -163dBc/Hz @ 1MHz offset and FOM (figure of merit) -212.4 dBc/Hz at 1MHz offset. The octave band VCO (1.2-2.4 GHz) shown in Figure (8) is best phase noise performance for a given power consumption, size, and Figure of merit.
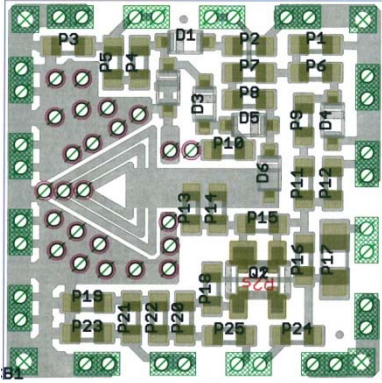

Fig.7. Layout of tunable oscillator using printed coupled resonator in stripline configuration
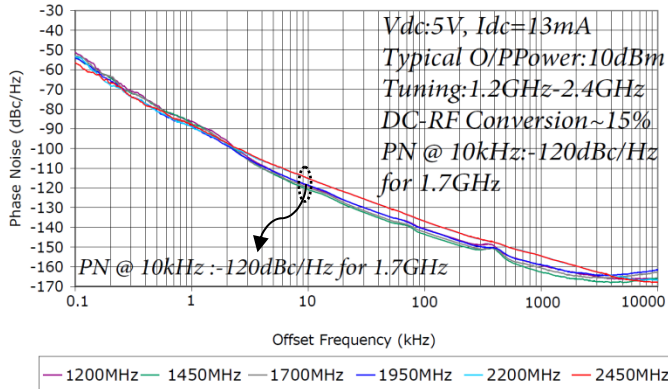

Fig. 8 Measured phase noise plot of stripline resonator oscillator (Fig. 7)

Table 1: Recent published tunable oscillator performance and this work

Ref.	f_o GHz	Tuning	P_o dBm	DC-RF Conversion Efficiency	$L(f)$ dBc/Hz @ 1MHz	FOM dBc/Hz @ 1MHz
[8]	10	1.2%	10	2%	-134.4	-187.4
[9]	8	0%	10	5%	-150	-205
[10]	8.2	1.28%	7	12.5%	-149.5	-211.7
[11]	9.9	20%	6	13.2%	-121.8	-187
This Work	1.2	100%	10	15.38%	-163	-212.4

B. Crystal Resonator

Reference frequency sources require high Q (quality factor) energy saving element such as crystal resonator for stable low phase noise operation. Figure (9) shows typical representation of crystal resonator, the first LCR branch (L_1, C_1, and R_1) represents fundamental modes (excited by the piezoelectric effect), C_0 is the holder capacitance, and the other branches (L_n, C_n, and R_n) are the odd overtone modes. The input impedance $Z(s)$ is given by [7]

$$Z(s) = \frac{1}{Y(s)} = \frac{s^2 + sR_i/L_i + 1/L_iC_i}{sC_0[s^2 + sR_i/L_i + (C_0 + C_i)/L_iC_iC_0]} = \frac{(s - s_{z1})(s - s_{z2})}{C_0(s - s_{p0})(s - s_{p1})(s - s_{p2})} \quad (18)$$

$$s_{z1,2} = -\frac{\omega_0}{2Q} \pm j\omega_0\sqrt{1 - \frac{1}{4Q^2}} \approx -\frac{\omega_0}{2Q} \pm j\omega_0, \quad for \quad Q \gg 1 \quad (19)$$

$$s_{p1,2} = -\frac{\omega_0}{2Q} \pm j\omega_0\sqrt{1 + \frac{C_i}{C_0} - \frac{1}{4Q^2}} \approx -\frac{\omega_0}{2Q} \pm j\omega_0\left(1 + \frac{C_i}{2C_0}\right) \quad (20)$$
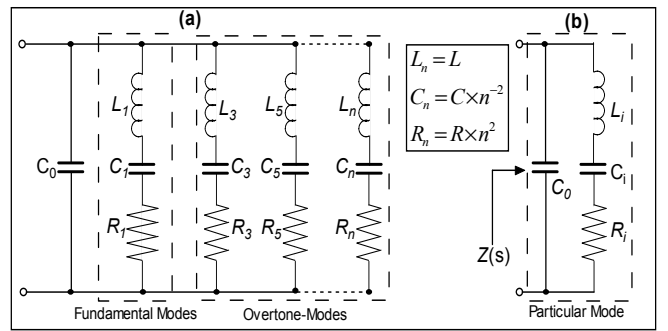

Fig.9: A typical electrical equivalent circuit of a quartz crystal

$$\omega_i = \frac{1}{\sqrt{L_iC_i}} \Rightarrow f_i(series) = \frac{1}{2\pi\sqrt{L_iC_i}}, \quad Q = \frac{L_i\omega_0}{R_i} = \frac{1}{R_iC_i\omega_0} \quad (21)$$

where $s_{z1,2}$ and $s_{p1,2}$ are zero and poles, f_i is the series resonance frequency and Q is the quality factor. One can represent the parallel resonance condition as

$$\omega_p \approx \omega_0\left(1 + \frac{C_i}{2C_0}\right)\Big|_{C_0 \gg C_i} \Rightarrow f_p(parallel) \approx \frac{1}{2\pi\sqrt{L_iC_i}}\left(1 + \frac{C_i}{2C_0}\right)\Big|_{C_0 > C_i} \quad (22)$$

$$m = \frac{2Q(\omega_p - \omega_0)}{\omega_0} = \frac{2Q(f_p - f_0)}{f_0}, \quad m \text{ is mode separation} \quad (23)$$

From (23), the intrinsic fluctuation in crystal influences the mode separation (m), and the degree to which crystal oscillator maintains a stable frequency f_i throughout a specified period of time is defined as the frequency stability of the source. The linear LCR crystal resonator model as shown in Figure (9) may give misleading phase noise data. Therefore, linear model is extended to nonlinear $L_{n,v}(t), C_{n,v}(t), R_{n,v}(t)$ drive level dependent model to address the intrinsic fluctuations of the crystal resonator components, where n stands for overtone mode and v (t) stands for drive level. The series resonance frequency of a crystal resonator is determined by series motional inductance $L_{n,v}(t)$ series capacitance $C_{n,v}(t)$; the changes in resonance frequency vary proportional to the square of the crystal current associated with the particular overtone mode. From [15], greater the value of dynamic capacitance $C_{n,v}(t)$, the higher the voltage-control sensitivity and poorer the phase noise performance. The dynmaic capacitance $C_{n,v}(t)$ can be expressed as stored mechanical energy. For small crystal current, the mechanical strain is little and the stored mechanical energy depends on first order elastic constant but

in reality this is not the case. Under large drive-level condition, crystal current becomes larger resulting in high mechanical strain. In this case, stored mechanical energy becomes function of higher order elastic constant, therefore $C_{n,v}(t)$ is dependent on higher order elastic constant and applied voltage [15]. The instantaneous value of equivalent circuit parameter of the nth branch of crystal resonator model as depicted in Figure (9) is a non-linear function of the total current thru the crystal, modulated by a random time-function formulated as a $1/f$-noise quantity in the frequency-domain [5].

For validation, 100MHz crystal resonator based Colpitts oscillator was designed according to a set of specifications that included +13 dBm output power, 50-Ω load, and phase noise of −132 dBc/Hz offset 100 Hz from the carrier, with the intention of applying the new approach to this basic design to determine the component parameters that mostly affect the phase noise performance for a given class and topology. For this typical design example, an NE68830 transistor from NEC was selected for the validation. The first step in the design process involved calculating the operating point for a fixed normalized drive of x = 20 (Table 6-1 in ref. 6). The output voltage and current at the fundamental frequency ($\omega_0 = 2\pi f_0$), based on the output-power requirement, can be given by

$$V_{out}(\omega_0) = \sqrt{P_{out}(\omega_0) * 2R_L} = \sqrt{20E-3*2*50} \approx 1.414V \quad (24)$$

$$I_{out}(\omega_0) = \frac{V_{out}(\omega_0)}{50} = \frac{1.414}{50} = 28.3mA \quad (25)$$

The DC operating point is calculated based on the normalized drive level x = 20. The expression for the emitter dc current can be found in terms of the Bessel function with respect to the drive level as [6]

$$[I_E(\omega_0)] = 2I_{DC}\left[\frac{I_1(x)}{I_0(x)}\right]_{x=Normalized-Drive-Level} \quad (26)$$

For the normalized drive level x = 20, the current distribution at DC and fundamental frequency (ω_0) are

$$[I_E(\omega_0)]_{x=20} = [I_{E1}(\omega_0)]_{x=20} + [I_{E2}(\omega_0)]_{x=20} = 2I_{DC}\left[\frac{I_1(x)}{I_0(x)}\right]_{x=20} \approx 56mA \quad (27)$$

$$[I_{E1}(\omega_0)]_{x=20} = I_{out}(\omega_0) = 28.3mA \text{ (O/P current to the load)} \quad (28)$$

$$[I_{E2}(\omega_0)]_{x=20} = [I_E(\omega_0)]_{x=20} - [I_{E1}(\omega_0)]_{x=20} = 27.3mA \quad (29)$$

$$I_{E-DC} = \frac{[I_E(\omega_0)]_{x=20}}{2\left[\frac{I_1(x)}{I_0(x)}\right]_{x=20}} = 28.3mA \quad (30)$$

The second step in the design process involved development of the biasing circuit. For the best close-in phase noise, a noise-feedback DC circuit is incorporated to provide the desired operating DC conditions with I_E = 28.3 mA, V_{CE} = 5.5 V, supply voltage, V_{cc} = 8 V, $\beta \approx 120$, and $I_B \approx 0.23$ mA.

The third step involves calculating the large-signal transconductance Y_{21} (see Tables 6-1 and 6-2 in ref. 6) as

$$Y_{21}|_{large-signal} = G_m(x) = \frac{qI_{dc}}{kTx}\left[\frac{2I_1(x)}{I_0(x)}\right]_{f=fundamental} \quad (31)$$

$$[Y_{21}]_{\omega=\omega_0} = \left[\frac{1.949I_{E-DC}}{520mV}\right] = 0.107 \quad (32)$$

The fourth step in the procedure involves the calculation of loop gain and equivalent loss resistance as

$$Loop-Gain = [LG]_{sustained-condition} = \left[\frac{R_{p1}(f_0)Y_{21}(x)}{n}\right] = \left[\frac{Rg_m}{x}\right]\left[\frac{2I_1(x)}{I_0(x)}\right]\left[\frac{1}{n}\right] > 1 \quad (33)$$

$$R_{p1}(f_0) = \text{Re}[Z_{11}] = 42.45\Omega \quad (34)$$

where $R_{p1}(f_0)$ is the equivalent resistive load across the port 1 (Fig. 11). For practical purpose, the loop gain should be 2.1 to achieve good starting conditions for stable and guaranteed oscillation. From (32) and (34)

$$n = \left[\frac{R_{P1}(f_0)Y_{21}(x)}{Loop-Gain}\right] = \frac{0.107 \times 42.45}{2.1} \approx 2.16 \quad (35)$$

The fifth step in the design procedure involves calculation of the feedback capacitor ratio as

$$n = 1 + \left[\frac{C_1}{C_2}\right] = 2.16 \Rightarrow \left[\frac{C_1}{C_2}\right]_{x=20} = 1.16 \quad (36)$$

The sixth step involves calculation of the absolute value of the feedback capacitor Z_{in} (looking into the base of the transistor) can be calculated as [1]

$$Z_{in} \cong -\left[\left(\frac{Y_{21}}{\omega^2(C_1^* + C_P)C_2}\right)\left(\frac{1}{(1+\omega^2 Y_{21}^2 L_P^2)}\right)\right] - j\left[\left(\frac{(C_1^* + C_P + C_2)}{\omega(C_1^* + C_P)C_2}\right) - \left(\frac{\omega Y_{21}L_P}{(1+\omega^2 Y_{21}^2 L_P^2)}\right)\left(\frac{Y_{21}}{\omega(C_1^* + C_P)C_2}\right)\right] \quad (37)$$

where C_P = (C_{BEPKG} +Contribution from layout)=1.1pF, L_P=(L_B + L_{BX} +Contribution from layout)=2.2nH.

The expression for the negative resistance (R_n, without parasitics) can be described by

$$R_{neq} = \frac{R_n}{(1+\omega^2 Y_{21}^2 L_P^2)} \cong \frac{R_n}{1.0218} \quad (38)$$

$$R_n = -\left[\frac{Y_{21}^+}{\omega^2 C_1 C_2}\right]_{x=20} = \frac{0.107}{(2\pi \times 1 \times 10^8)^2 C_1 C_2} \quad (39)$$

For sustained oscillation → $R_{neq} \geq 2R_{P1}(f_0) \cong 84.90$ Ω, $R_n \geq$ 1.0218×84.90 ≅ 86.76 Ω . From (33) and (39),

$$C_1 C_2 \leq \left[\frac{1}{(2\pi \times 1 \times 10^8)^2}\right]\left[\frac{0.107}{86.76}\right] \approx 3.13 \times 10^{-21} \quad (40)$$

$$C_1 = 25pF = [C_1^* + C_P] \Rightarrow C_1^* = C_1 - C_P = 23.84pF, \quad C_2 = 22pF \quad (41)$$

For practical purpose, C_1^* =22pF. The seventh step is to determine noise factor (F), which is needed apriori for the evaluation of the phase noise. Figure (10) shows the typical simplified Colpitts oscillator circuit including noise contributions. The expression of noise factor F and phase noise in dBc/Hz £(ω) in terms of the oscillator feedback component (C_1 and C_2) for the circuit shown in Figure (10) can be described by [6]

$$F = 1 + \frac{C_2 C_c}{(C_1 + C_2)C_1 r_e}\left[r_b + \frac{1}{2r_e\beta}\left(r_b + \frac{(C_1+C_2)C_1 r_e}{C_2 C_c}\right)^2 + \frac{r_e}{2} + \frac{1}{2r_e}\left(r_b + \frac{(C_1+C_2)C_1 r_e}{C_2 C_c}\right)^2\left(\frac{f^2}{f_T^2}\right)\right] \quad (42)$$

$$£(\omega) = 10Log\left(\left(4kTR_L + \frac{4qI_c g_m^2 + \frac{K_f I_b^{AF}}{\omega}g_m^2}{\omega_0^2 C_1^2(\omega_0^2(\beta^+)^2 C_2^2 + g_m^2 \frac{C_2^2}{C_1^2})}\right)\left[\frac{\omega_0^2}{4\omega^2 V_{cc}^2}\right]\left[\frac{Q_u^2}{Q_L^2} + \frac{[C_1+C_2]^2}{C_1^2 C_2^2 \omega_0^4 L^2 Q_L^2}\right]\right) \quad (43)$$

$$\beta^+ = \left[\frac{Y_{21}^+}{Y_{11}^+}\right]\left[\frac{C_1}{C_2}\right]^p; \quad g_m = [Y_{21}^+]\left[\frac{C_1}{C_2}\right]^q \quad (44)$$

where Y_{21}^+, Y_{11}^+ is the large signal [Y] parameter of the active device, K_f is the flicker noise coefficient, AF is the flicker noise exponent, R_L is the equivalent loss resistance of the tuned resonator circuit, I_c is the RF collector current, I_b is the RF base current, V_{cc} is the RF collector voltage, C_1, C_2 is the feedback capacitor (Fig. 5), Q_u and Q_L are unloaded and loaded

Q factors, p and q are the drive level dependent constants across base-emitter of the device [6]. The final step in this approach involves calculating the phase noise. From (42) and (43), the calculated phase noise at 100 Hz offset from the carrier frequency 100 MHz is -132 dBc/Hz (Q=100,000). The oscillator circuit shown in Figure (11) incorporates the component values as per above design calculations.

Figure (12) shows the CAD simulated phase noise and output power for 100 MHz crystal oscillators. Simulated and calculated data agrees within 2-3 dB. In a Colpitts oscillator configuration (Fig. 11) with quartz crystal resonator, a capacitive voltage divider is used and the crystal acts like a high-Q inductor, slightly detuned from its series resonant condition. Since quartz crystal is a mechanical resonator driven by the piezoelectric effect, fundamental and a variety of overtone frequency modes (3rd, 5th, 7th, 9th, and so on) are possible. Unfortunately, undesired mode jumping is also possible even in well-planned circuit designs. This problem can be overcome by mode-feedback mechanism (Fig. 14) that not only improves the stability but also improves the phase noise performances by 10-15 dB. In addition to this, the dynamic phase-injection and mode-coupling approach shown in Figure (14) enhances the dynamic loaded Q, and to reduce or eliminate phase hits, while reducing the thermal drift and susceptibility to microphonics to an extremely low level, and retaining low phase noise and broadband tunability.

III. EXAMPLE: POWER EFFICIENT 100MHz SIGNAL SOURCE

Figure (14) shows the 5th overtone 100 MHz crystal oscillator, utilizing dynamic phase-injection and mode-coupling improves the phase noise and stability].
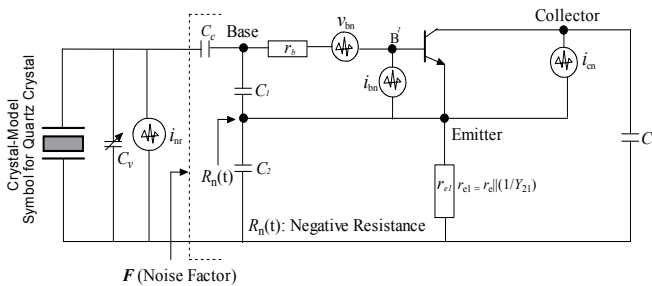

Fig.10. Typical Colpitts oscillator circuit including noise contribution
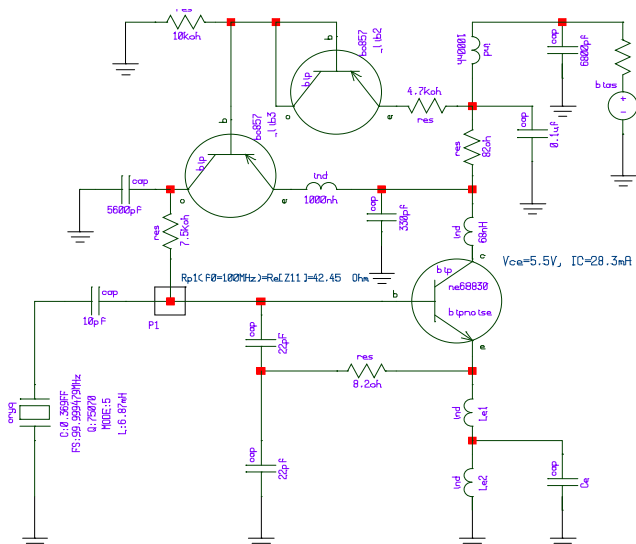

Fig.11. 100MHz crystal oscillator (tuning diodes are not included for simplification)
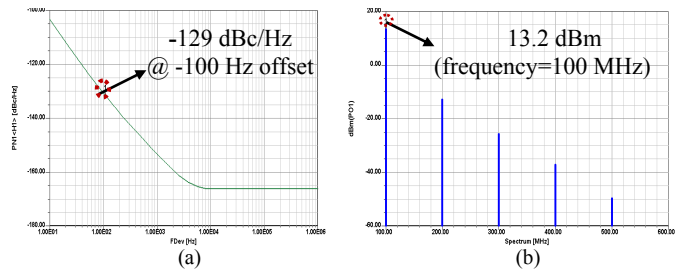

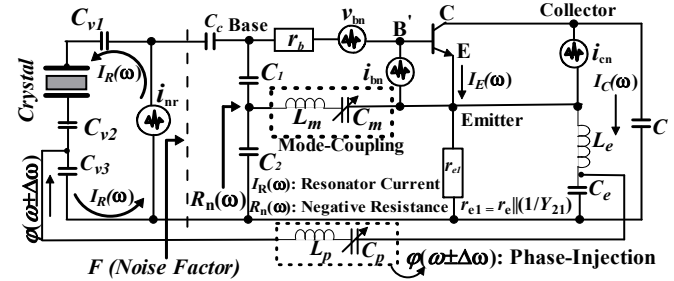Fig.12. Simulated plot of 100 MHz oscillator :(a) PN, and (b) O/P power

Fig.13. A typical mode-coupled phase-injected $\varphi(\omega \pm \Delta\omega)$ crystal oscillator, including noise contributions (transistor and resonator)

As shown in Figure (14), higher order mode is coupled through output path and feedback to the point where resonator impedance shows steep change of phases, thereby, maximization of group delay. Figure (15) shoes the DUT (device under test: 100MHz OCXO) connected with phase noise measurement equipment. The dynamic PI (phase-injection) is an effective method to reduce the $1/f$ noise. By introducing MC (mode-coupling) close-in noise is reduced by an additional of approximately 10-15 dB in the flicker region. Figures (16) and (17) show the CAD simulated and measured phase noise plots for comparative analysis, with crystal resonator unloaded quality factor of 100,000.
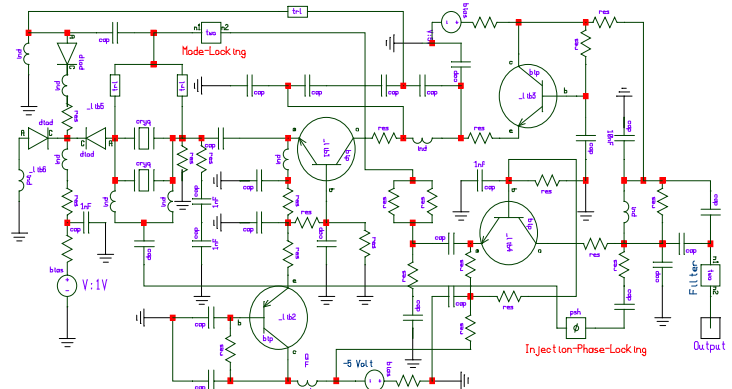

Fig.14. 100 MHz 5th overtone crystal oscillator circuit (DC Bias: 5V, 42mA), heater circuit is not included, typical power consumption in steady-state with heater is typically 660mW, startup power consumption with heater 1120 mW)
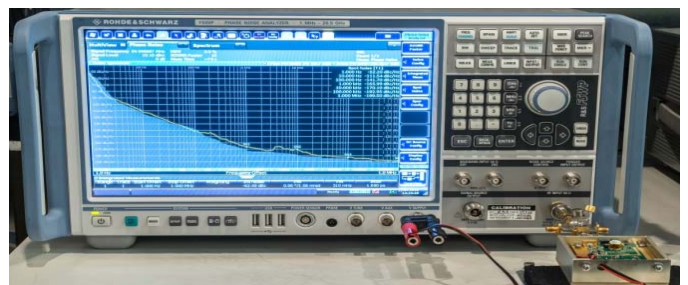

Fig.15. Shows the measurement setup with 100 MHz 5th overtone OCXO, the measured PN is -141dBc/Hz @ 100Hz offset with -193 dBm/ Hz noise floor
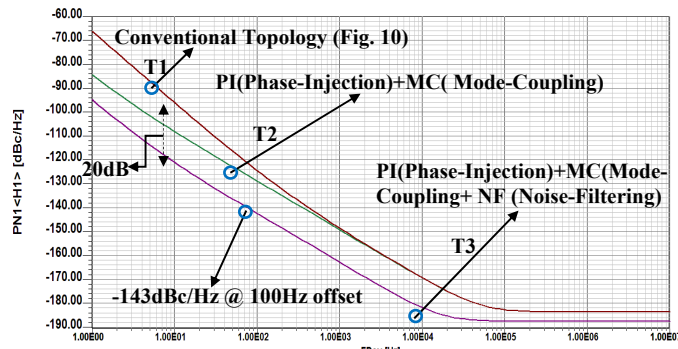
Fig.16. CAD simulated PN plots for 100 MHz 5th overtone OCXO (ovenized crystal oscillator): trace T1, T2, and T3 show the conventional 100 MHz OCXO, MC+NF (mode-coupled and noise filtering), and PI+MC+NF (phase-injection, mode-coupled, and noise filtering), noise floor of trace T3 is -190 dBm/Hz@ 1MHz offset

As shown in Figure (16), minimization of noise performance at far offset (>100 kHz) is achieved by adaptive self-tuning noise filtering network. As illustrated in Figures (15) and (16), noise filtering offers significant improvement in noise floor. Figure (17) shows the measured phase noise plots, measurement closely agree with CAD simulated phase noise depicted in Figure (16). The measured phase noise performance at 100 Hz offset from the 100 MHz carrier is -140.83dBc/Hz with 16.22 dBm output power. The far offset measured noise floor is -189.85dBm/Hz at 1MHz offset. The total power consumption in steady state is 660mW (210 mW for crystal resonator oscillator + 350mW for ovenized heater). The total startup DC power consumption is 1120 mW that includes heater and oscillator circuit. The measured FOM (figure of merit) is -235.8 dBc/Hz at 1 kHz offset for 100MHz ovenized crystal resonator oscillator. The crystal circuit (Fig. 14) exhibits PN -169 dBc/Hz and FOM -245.7dBc/Hz @ 1kHz offset with 15.7dBm o/p power and DC-RF conversion efficiency17.69 % when heating circuit is not connected, Table 2 shows the recent published papers on crystal resonator oscillators, compares this work based on DC-RF conversion efficiency, PN and FOM at 1 kHz offset from the carrier.
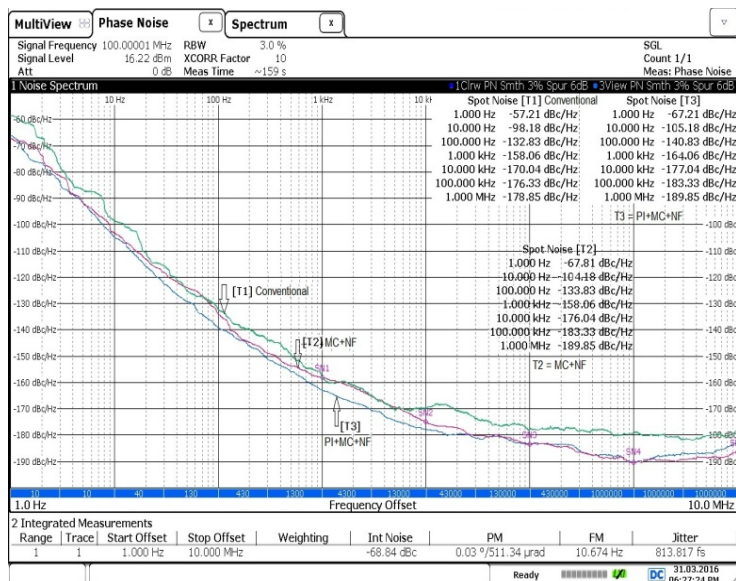

Fig.17. Measured PN plots for 100 MHz 5th overtone OCXO: trace T1, T2, and T3 show the conventional 100 MHz OCXO, MC+NF (mode-coupled and noise filtering), and PI+MC+NF (phase-injection, mode-coupled, noise filtering), noise floor of trace T3 is -189.85dBc/Hz@ 1MHz offset

Table 2: Recent published Crystal oscillator performance and this work

References	f_o MHz	P_{DC} mW	P_o dBm	DC-RF Conversion Efficiency	$L(f)$ dBc/Hz @ 1kHz	FOM dBc/Hz @ 1kHz
[17]	80	250	15.4	13.8%	-164	-238
[18]	100	300	7.9	2.05%	-157	-232.2
[19]OCXO With heater	100	1000	3.98	3.98%	-163	-233
This Work OCXO With heater	100	660	16.22	6.31%	-164	-235.8
This Work Without heater	100	210	15.7	17.69%	-169	-245.7

(Ref. 17 and 18 shown in Table 2 describes crystal oscillator without heater.)

IV. CONCLUSION

This work offers a new criterion for designing power-efficient signal sources, reported novel approach PI (phase-injection) and ML (mode-locking) techniques can be applied for other variation of oscillators circuits.

REFERENCES

[1] US 1624537, Colpitts, Edwin H, "Oscillation generator", published 1 February 1918, issued 12 April 1927

[2] F. A. Record and J. L. Stiles,"An Analytical Demonstration of Hartley Oscillator Action",, Proceedings of the IRE 31 (6), 1943.

[3] J. K. Clapp, "An inductance-capacitance oscillator of unusual frequency stability", Proc. IRE, vol. 367, pp. 356-358, Mar. 1948

[4] A. K. Poddar, "Slow Wave Resonator Based Tunable Multi-Band Multi-Mode Injection-Locked Oscillator" Dr.-Ing.-habil Thesis, BTU Cottbus, Germany, 2014 (https://opus4.kobv.de/opus4-btu/frontdoor/index/index/docId/3193)

[5] A. K. Poddar and U. L. Rohde, "Techniques Minimize the Phase Noise in Crystal Oscillators", 2012 IEEE FCS, pp. 01-07, May 2012.

[6] Ulrich L. Rohde, Ajay K. Poddar, Georg Böck, "The Design of Modern Microwave Oscillators for Wireless Applications ", John Wiley & Sons.

[7] A. K. Poddar and U. L. Rohde, "Crystal Oscillators" and Crystal Oscillator Design", Wiley Encyclopedia and Electro. Engg.", Oct. 2012.

[8] Y.-T. Lee, 1. Lee, and S. Nam, "High-Q active resonators using amplifiers and their applications to low-phase noise freerunning and voltage-controlled oscillators," IEEE Trans. MTT, vol. -52, no. 11, pp. 2621-2626, Nov., 2004.

[9] M. Nick, and A. Mortazawi, "Oscillator phase-noise reductionusing low-noise high-q active resoantors," in IEEE MTT -S Int.Microwave Symp. Dig., May 2010, pp. 276-279.

[10] M. Nick, A. Mortazawi, "A very low phase-noise voltage-controlled-oscillator at X-band",IEEE MTT-S Digest, pp. 1-4, 2011

[11] E. Turkmen et al, " The X (Band) Files: An X-band Microstrip Voltage-Controlled Oscillator with Wideband Tuning", IEEE Microwave Magazine, Vol. 17, PP. 88-93, Jan 2016

[12] S. Jain et. al, "Tuned LC-Resonator Dual-Band VCO", IEEE MWCL Letters, Vol. 26, No. 3, pp. 204-206, March 2016

[13] F. Thome et. al, "Prospects and Limitations of Stacked-FET Approaches for Enhanced Output Power in Voltage-Controlled Oscillators", IEEE Trans. on MTT, Vol. 64, No. 3, pp. 836-846, March 2016.

[14] J.-Hoon Song, B.-Sung Kim, S. Nam, "An Adaptively Biased Class-C VCO With a Self-Turn-Off Auxiliary Class-B Pair for Fast and Robust Startup", IEEE MWCL, Vol. 26, No. 1, pp. 34-36, Jan 2016

[15] T. Yasuda et al., Nonlinear model of crystal resonator and its application to phase noise simulator of oscillator", IEEE IFCS. pp. 1-3, May 2014

[16] Y. Vorokhovsky et al., Recent achievements in performance of 100 MHz crystals and OCXOs", EFTF, pp. 367-369, 2014

[17] X. Huang et al, "Prediction, simulation, and verification of the phase noise in 80-MHz Low-Phase-Noise Crystal Oscillators", IEEE Transaction on UFFC, vol. 62, No. 9, pp. 1599-1604, Sept. 2015

[18] X. Huang, D. Liu, Y. Wang, P. Chen, and W. Fu", 100-MHz Low-Phase-Noise microprocessor temperature compensated crystal oscillator", IEEE Trans. on Circuits and Systems-II, Express Briefs, vol. 62, No. 7, pp. 636-640, July 2015.

[19] R. Boroditsky, J. Gomez, " Micro minature, SMD, Ultra low phase noise, high frequency OCXO", EFTF, pp. 360-362, 2014.